AIAA JOURNAL
Vol. 34, No. 11, November 1996

Computation of Quadrupole Noise Using Acoustic Analogy

Meng Wang,* Sanjiva K. Lele,† and Parviz Moin‡
Stanford University, Stanford, California 94305

Acoustic analogy computations of vortex shedding noise were carried out in the context of a two-dimensional, low-Mach-number laminar flow past a NACA 0012 airfoil at chord Reynolds number of 10^4. The incompressible Navier–Stokes equations were solved numerically to give an approximate description of the near-field flow dynamics and the acoustic source functions. The radiated far-field noise was computed based on Curle's extension to the Lighthill analogy. This study emphasizes an accurate evaluation of the Reynolds stress quadrupoles in the presence of an extensive wake. An effective method for separating the physical noise source from spurious boundary contributions caused by eddies crossing a permeable computational boundary is presented. The effect of retarded-time variations across the source region is also examined. Computational solutions confirm that the quadrupole noise is weak compared with the noise due to lift and drag dipoles when the freestream Mach number is small. The techniques developed in this study are equally applicable to flows in which the volume quadrupoles act as a prominent noise source.

Nomenclature

C = airfoil chord
c = sound speed
c_q = boundary correction to p_q
D_i = surface dipole source function
M = freestream Mach number
n_i = unit outward normal to solid surface S
p = fluid pressure
p_{ij} = compressive stress tensor
p_q = acoustic pressure due to quadrupole radiation
Q_{ij} = volume quadrupole source function
Re = chord Reynolds number
r = separation between source and observation points, $r = |\boldsymbol{x} - \boldsymbol{y}|$
S = airfoil surface
S_0 = exit surface for source integration
T_{ij} = Lighthill stress tensor
t = time
U_c = eddy convection velocity
u_i = fluid velocity in x_i direction
V = source integration volume
V_0 = truncated source integration volume
v_i = fluid velocity relative to freestream
$\boldsymbol{x}$ = far-field position vector
x_i = Cartesian coordinates
$\boldsymbol{y}$ = source field position vector
α = angle of attack
γ = ratio of specific heats
δ_{ij} = Kronecker delta
θ = angle from x_1 axis
ρ = fluid density
ρ_q = acoustic density due to quadrupole radiation
τ_{ij} = viscous stress tensor
ω = vorticity; circular frequency
$()_\infty$ = freestream quantity
$()'$ = dimensional quantity
$\hat{()}$ = quantity in frequency domain

Received Jan. 10, 1996; revision received May 14, 1996; accepted for publication June 18, 1996; also published in *AIAA Journal on Disc*, Volume 2, Number 1.

*Research Associate, Center for Turbulence Research, Stanford University/NASA Ames Research Center, MS 202A-1, Moffett Field, CA 94035.
†Assistant Professor, Department of Aeronautics and Astronautics and Department of Mechanical Engineering. Member AIAA.
‡Franklin and Caroline Johnson Professor of Engineering, Department of Mechanical Engineering; also Senior Staff Scientist, NASA Ames Research Center, Moffett Field, CA 94035. Associate Fellow AIAA.

I. Introduction

THE objective of this investigation is to develop useful techniques of computational aeroacoustics based on acoustic analogy theory. The vortex shedding noise generated by a two-dimensional laminar flow past a NACA 0012 airfoil is used as a paradigm to examine a number of important numerical aspects, particularly with regard to the accurate evaluation of volume-distributed quadrupoles. The issues addressed include the elimination of the spurious boundary noise caused by eddie structures crossing a computational boundary and the adequate treatment of finite retarded-time variations across a source region.

The prediction of flow-induced noise is facilitated tremendously by the acoustic analogy theories pioneered by Lighthill.[1] By recasting the exact equations of fluid motion into a linear, inhomogeneous wave equation, Lighthill demonstrates that an unsteady flow region in an unbounded fluid is acoustically equivalent to a distribution of quadrupole sources, which produce a radiated acoustic intensity proportional to the eighth power of the disturbance velocity. In the limit of low Mach number and compact vorticity region, the Lighthill analogy has been validated in the sense of matched asymptotic expansions,[2] as well as direct numerical simulation.[3]

Acoustic analogies can be applied in conjunction with direct numerical simulation or large eddy simulation of source fields to provide effective means of computational aeroacoustics. The procedure, sometimes called the hybrid approach, is particularly attractive for low-Mach-number flows, characterized by vast disparities between the hydrodynamic near field and the acoustic far field in terms of length scales as well as energy density, because the expensive Navier–Stokes simulation is limited to the hydrodynamic quantities in a relatively small source region. Recent applications of the hybrid technique include studies of axisymmetric jet noise,[4,5] boundary-layer transition noise,[6] and the noise of isotropic turbulence.[7]

In many flows of practical interest, such as jets and wakes, the hydrodynamic source region decays very slowly in the downstream direction. Artificial outflow (and sometimes inflow) boundaries have to be placed to limit the computational domain size. A crucial yet frequently overlooked difficulty in acoustic analogy calculations is the effect of eddies exiting from (or entering into) the source integration domain through these artificial boundaries. The escaping eddies generate spurious, powerful signals that contaminate severely the acoustic field.[8] An analogous difficulty exists in the direct computation of sound using Euler or compressible Navier–Stokes equations, and there the formulation of nonreflective boundary conditions has been a subject of extensive study.[9] A major emphasis of the present work is to explore techniques capable of isolating the physical noise

source from the spurious boundary contributions in an acoustic analogy calculation. A corrective formula accounting for the unsteady momentum fluxes associated with the escaping eddies is developed, which is shown to generate satisfactory results.

When a solid body is present in the flow, Curle's integral solution[10] to the Lighthill equation provides a theoretical framework for predicting the noise of flow-body interaction. It predicts powerful dipole radiation as a result of the fluctuating stresses acting on the fluid by the solid boundaries, in addition to the quadrupole sound caused by the unsteadiness of the fluid itself. Among the applications of the Curle integral are the predictions of aeolian tones[11] and, more recently, the noise of flows past an airfoil[12] and a delta wing.[13] In the latter two studies, the Navier–Stokes equations are solved numerically in the near field to provide the unsteady lift and drag forces on the airfoil (wing) surface and hence the acoustic dipole strength. The acoustic quadrupoles are neglected on the basis of low Mach number. A generalization to the Curle solution, incorporating the effect of arbitrary source motion, has been derived by Ffowcs Williams and Hawkings.[14]

In the present study, an unsteady, two-dimensional laminar flow past a NACA 0012 airfoil is used to generate aeroacoustic dipole and quadrupole sources. Under the low-Mach-number approximation, the near-field flow quantities are obtained by solving the incompressible Navier–Stokes equations numerically at chord Reynolds number of 10^4. Periodic as well as aperiodic vortex shedding, depending on the angle of attack, is established near the airfoil trailing edge.

The far-field noise is computed using Curle's integral formulation of the Lighthill analogy.[10] The boundary correction technique, mentioned earlier, allows an accurate evaluation of the Reynolds stress quadrupoles, in addition to the more readily computable lift and drag dipoles on the airfoil surface. The effect of slightly noncompact source distribution with full account of retarded-time variations is assessed by comparisons with the compact source solutions. The numerical results confirm, in quantitative terms, that the far-field sound is dominated by the surface pressure dipoles at low Mach number. The emphasis of this work is, however, to present a methodology for the accurate evaluation of acoustic quadrupoles from flow simulation data. The techniques are applicable to a wide range of flows, including jets and mixing layers, in which the Reynolds stress quadrupoles play a prominent or even dominant role in the overall sound generation.

II. Flow Simulation

We consider the unsteady flowfield and the sound generated by a NACA 0012 airfoil placed in a two-dimensional uniform flow. The Reynolds number, defined as $Re = U'_\infty C'/\nu'$, where U'_∞, C', and ν' denote the (dimensional) freestream velocity, the chord, and the kinematic viscosity of the fluid, respectively, is equal to 10^4. The freestream Mach number $M < O(1)$, where $M = U'_\infty/c'_\infty$ and c'_∞ is the sound speed. The airfoil angle of attack is $\alpha = 5$ deg for most acoustic calculations to be presented, although the case of $\alpha = 8$ deg is also considered.

In the spirit of Lighthill's analogy, the acoustic source functions can be determined from an incompressible flow approximation, given that the compressibility effect is of $O(M^2)$, or $\rho \equiv \rho'/\rho'_\infty = 1 + O(M^2)$. Thus, in the near field the dimensionless equations of mass and momentum conservation reduce to

$$\frac{\partial u_i}{\partial x_i} = 0 \tag{1}$$

$$\frac{\partial u_i}{\partial t} + u_j \frac{\partial u_i}{\partial x_j} = -\frac{\partial p}{\partial x_i} + \frac{1}{Re}\frac{\partial^2 u_i}{\partial x_j \partial x_j} \tag{2}$$

for $i = 1$ and 2, where $u_i = u'_i/U'_\infty$, $x_i = x'_i/C'$, $p = p'/(\rho'_\infty U'^2_\infty)$, and $t = t'U'_\infty/C'$. A finite difference code developed by Choi[15] is used to solve Eqs. (1) and (2) numerically in a generalized coordinate system. Second-order central difference is used for spatial discretization on a staggered grid. The time advancement is of the fractional-step type, in combination with the Crank–Nicolson method for viscous terms and the third-order Runge–Kutta method for convective terms. The continuity requirement (1) is imposed through a pressure Poisson equation, which is solved using a multigrid iterative procedure.

Computations are carried out on a C-type mesh configuration shown in Fig. 1, where only one-quarter of the mesh lines are plotted for clarity. A total of 896 × 104 mesh cells are used in the simulations, run with a time step $\Delta t = 2.3 \times 10^{-3}$. No-slip velocity conditions are imposed on the airfoil surface. Along the C-shaped outer boundary, the velocities are fixed at the freestream values, $u_i = (1, 0)$. Because the boundary is sufficiently far (~3 chords) away from the airfoil, this approximation should have little impact on the solution behavior. At the downstream boundary a convective outflow condition of the type used by Pauley et al.[16] is applied to allow the vortical disturbances in the wake to leave the computational domain smoothly.

Simulations start with uniform velocity $u_i(t = 0) = (1, 0)$ everywhere. During the initial transient period, a starting vortex is shed at the trailing edge, and boundary layers develop on the upper and lower surfaces. The upper-surface boundary layer soon separates. It interacts with the lower boundary layer near the trailing edge to develop a periodic vortex shedding pattern for $\alpha = 5$ deg, as illustrated in Figs. 2a and 2b. Figure 2a depicts contours of the streamwise velocity u_1 at a given time $t = 24.5$, and Fig. 2b depicts contours of the corresponding negative vorticity $-\omega$. The vortices shed from the lower layer (positive vorticity) are seen to be more intense than their upper-layer counterparts (negative vorticity).

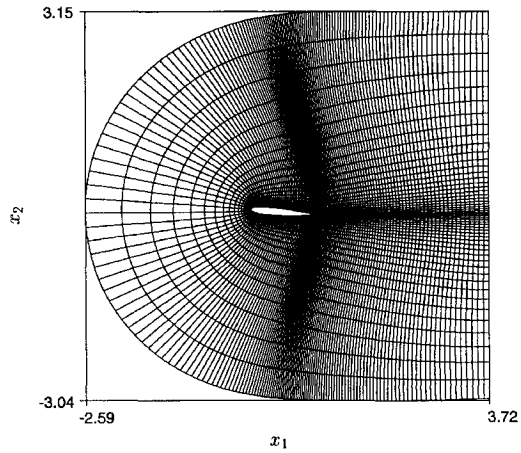

Fig. 1 Computational mesh for flow past a NACA 0012 airfoil at $\alpha = 5$ deg. For clarity only one in every four mesh lines is plotted.

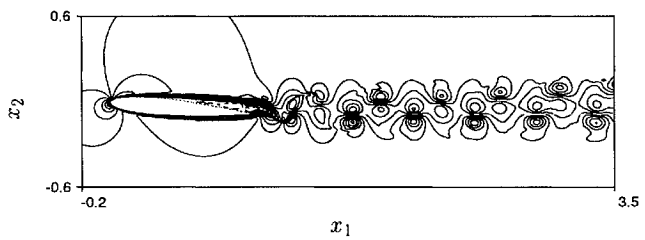

a) Streamwise velocity u_1

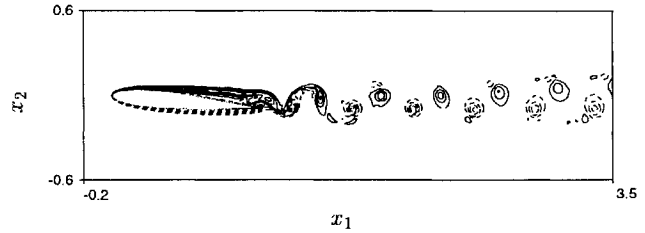

b) Negative vorticity $-\omega$

Fig. 2 Contours for a two-dimensional laminar flow past a NACA 0012 airfoil at 5 deg angle of attack, at $t = 24.5$. The chord Reynolds number is 10^4. Contour levels: a) −0.35–1.45, increment 0.10; and b) −308.0–804.0, increment 8.0.

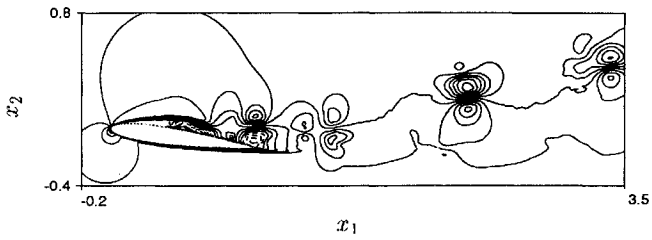

a) Streamwise velocity u_1

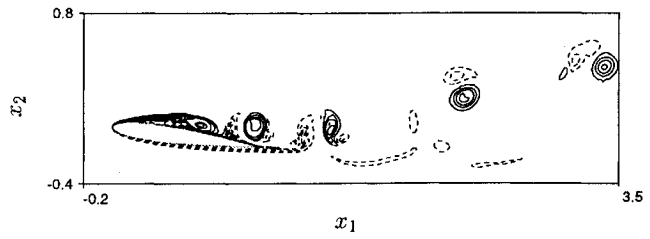

b) Negative vorticity $-\omega$

Fig. 3 Contours for a two-dimensional laminar flow past a NACA 0012 airfoil at 8 deg angle of attack, at $t = 26.8$. The chord Reynolds number is 10^4. Contour levels: a) −0.90–2.10, increment 0.20; and b) −335.0–1175.0, increment 10.0.

Figures 3a and 3b again plot contours of the streamwise velocity and negative vorticity, respectively, for a higher angle of attack $\alpha = 8$ deg, at $t = 26.8$. In this case the vortex shedding process, initiated by the instability of the separated upper shear layer near the midchord, is aperiodic. The unsteady lift and drag coefficients exhibit aperiodic, perhaps chaotic oscillations with time even after an extended time lapse (~30 chord flow-through times). Similar behavior has been observed and analyzed by Pulliam[17] using the concept of nonlinear dynamics.

III. Aeroacoustic Theory

The density fluctuation due to acoustic wave propagation from the aerodynamic source region is governed by the convected wave equation[18]

$$\left[\left(\frac{\partial}{\partial t}+\frac{\partial}{\partial x_1}\right)^2-\frac{1}{M^2}\frac{\partial^2}{\partial x_j\partial x_j}\right]\rho=\frac{\partial^2 T_{ij}}{\partial x_i\partial x_j} \tag{3}$$

where

$$T_{ij}=\rho v_i v_j+\delta_{ij}[p-(\rho/M^2)]-\tau_{ij} \tag{4}$$

is the Lighthill stress tensor defined in terms of the fluctuating velocity relative to the free-stream value, $v_i = u_i - \delta_{i1}$, and

$$\tau_{ij}=\frac{1}{Re}\left(\frac{\partial v_i}{\partial x_j}+\frac{\partial v_j}{\partial x_i}-\frac{2}{3}\delta_{ij}\frac{\partial v_k}{\partial x_k}\right) \tag{5}$$

is the viscous part of the Stokes stress tensor. The usual summation convention applies for repeated subscripts, and δ_{ij} is the Kronecker delta. Like the Lighthill equation, Eq. (3) is an exact restatement of the mass and momentum conservation equations for a compressible fluid. The use of relative velocity in the source function ensures that the Lighthill stress, predominantly the fluctuating Reynolds stress, is quadratically small outside the source region in the freestream. One notices that, because the radiated acoustic field has a characteristic spatial scale of M^{-1} times the hydrodynamic length scale, the two spatial derivative terms on the left-hand side of Eq. (3) are of $O(M)$ and $O(1)$, respectively, relative to the time derivative term.

Ffowcs Williams and Hawkings[14] derived a general solution for noise produced by a rigid surface moving through a quiescent medium. An exact solution to Eq. (3) is most easily obtained by rewriting the Ffowcs Williams–Hawkings equation in terms of the reception coordinates, i.e., in a reference frame moving with the body. For low-Mach-number flows, however, the bulk convective effect can be ignored to first approximation, and the simpler solution owing to Curle[10] prevails. If $\boldsymbol{x}$ and $\boldsymbol{y}$ are used to denote the position vectors of an observation point and a source element, respectively, and $\boldsymbol{r} = \boldsymbol{x} - \boldsymbol{y}$ and $r = |\boldsymbol{r}|$, Curle shows that

$$\rho(\boldsymbol{x},t)-1=-\frac{M^2}{4\pi}\frac{\partial}{\partial x_i}\int_S\frac{n_j p_{ij}(\boldsymbol{y},t-Mr)}{r}d^2\boldsymbol{y}+\frac{M^2}{4\pi}\frac{\partial^2}{\partial x_i\partial x_j}\int_V\frac{T_{ij}(\boldsymbol{y},t-Mr)}{r}d^3\boldsymbol{y} \tag{6}$$

for a rigid body at rest. In the preceding equation $p_{ij} = p\delta_{ij} - \tau_{ij}$ and n_i is the directional cosine of the outward normal (into the fluid) to the rigid surface S over which the surface integration takes place. The volume integral is taken over the entire unsteady flow region V external to the body. In the acoustic far field defined by $r \gg l_e/M$, where l_e is the typical eddy size, Eq. (6) simplifies to a form most suitable for numerical evaluation,

$$\rho(\boldsymbol{x},t)-1\approx\frac{M^3}{4\pi}\frac{\partial}{\partial t}\int_S\frac{r_i}{r^2}n_j p_{ij}(\boldsymbol{y},t-Mr)d^2\boldsymbol{y}+\frac{M^4}{4\pi}\frac{\partial^2}{\partial t^2}\int_V\frac{r_i r_j}{r^3}T_{ij}(\boldsymbol{y},t-Mr)d^3\boldsymbol{y} \tag{7}$$

Furthermore, if both the body (airfoil) and the unsteady flow region are small compared with the typical acoustic wavelength l_e/M, the source region is acoustically compact. The far-field density can be approximated by

$$\rho(\boldsymbol{x},t)-1\approx(M^3/4\pi)\left(x_i/|\boldsymbol{x}|^2\right)\dot{D}_i(t-M|\boldsymbol{x}|)+(M^4/4\pi)\left(x_i x_j/|\boldsymbol{x}|^3\right)\ddot{Q}_{ij}(t-M|\boldsymbol{x}|) \tag{8}$$

where

$$\dot{D}_i(t)=\frac{\partial}{\partial t}\int_S n_j p_{ij}(\boldsymbol{y},t)d^2\boldsymbol{y} \tag{9}$$

$$\ddot{Q}_{ij}(t)=\frac{\partial^2}{\partial t^2}\int_V T_{ij}(\boldsymbol{y},t)d^3\boldsymbol{y} \tag{10}$$

are, respectively, point dipole and quadrupole sources, representative of compact surface and volume sound radiation.

IV. Exit Boundary Correction

In the application of Curle's integral solution, the surface integral, taken over the finite airfoil surface, is well defined. The same cannot be said, however, regarding the volume integral. As illustrated in Figs. 1–3, the unsteady flow region is truncated in the wake by the artificial computational boundary. At the outflow boundary the Lighthill stress terms are significant, and their sudden termination there is known to cause strong, spurious acoustic sources.[8] The same difficulty has been encountered by Mankbadi et al.[5] and Mitchell et al.[4] in jet noise calculations. Mitchell et al.[4] employed model extensions that allow the Lighthill source terms to decay to zero slowly downstream of the computational domain. In the subsequent analysis we illustrate a simple, more systematic boundary correction procedure in which only the information at the outflow boundary is required.

The rationale for outflow boundary correction is based on the observation that, despite the apparently large unsteady region that extends beyond the computational domain, the primary physical source of sound, associated with specific events such as the vortex generation and shedding process in the present case or the vortex pairing in Ref. 4, is captured within the domain. Downstream of the vortex shedding region, the eddy motions are dominated by convection and are thus acoustically inefficient. The boundary correction formula is derived most easily by considering compact volume sources evaluated in two domains of integration, whose boundaries coincide except at the downstream exits. The exit boundaries are set to be Δy_1 apart (notice that the boundaries of source integration do not need to be identical to that of the near-field flow simulation). If $\dot{Q}_{ij}^{+}$ and $\dot{Q}_{ij}^{-}$ are used to denote the first time derivative

of the Lighthill stress integrals evaluated in the larger and smaller domains, respectively, one can deduce that

$$\dot{Q}_{ij}^{+}(t) \approx \dot{Q}_{ij}(t) + E_{ij}[t - (\tau/2)] \tag{11}$$

$$\dot{Q}_{ij}^{-}(t) \approx \dot{Q}_{ij}(t) + E_{ij}[t + (\tau/2)] \tag{12}$$

The common term in the two equations, $\dot{Q}_{ij}(t)$, represents the physical noise source situated within both domains, and function E_{ij} represents the boundary error caused by eddies escaping from the exit boundary. Because the separation between the two boundaries is very small, an eddy can be considered frozen as it traverses the distance Δy_1, and hence the error terms in (11) and (12) differ only by a small phase difference $\tau = \Delta y_1 / U_c$, where U_c is the local eddy convection velocity. Phase shifting (11) and (12) by $\tau/2$ and $-\tau/2$, respectively, and subtracting the latter equation from the former yield

$$\dot{Q}_{ij}[t + (\tau/2)] - \dot{Q}_{ij}[t - (\tau/2)] = \dot{Q}_{ij}^{+}[t + (\tau/2)] - \dot{Q}_{ij}^{-}[t - (\tau/2)] \tag{13}$$

or

$$\ddot{Q}_{ij}(t) \approx \tfrac{1}{2}\left[\ddot{Q}_{ij}^{+}(t) + \ddot{Q}_{ij}^{-}(t)\right] + (1/\tau)\left[\dot{Q}_{ij}^{+}(t) - \dot{Q}_{ij}^{-}(t)\right] \tag{14}$$

after a Taylor series expansion to $O(\tau^2)$. The first term on the right-hand side of (14) is the algebraic average of the quadrupole sources calculated from the two integration domains, whereas the second term clearly represents the desired correction at the exit boundary. Note that the correction term involves only the first time derivative, in contrast to the second time derivative in the original source terms. In the numerical implementation, Δy_1 should take the smallest possible value (one mesh spacing) to ensure the validity of the frozen-eddy assumption.

Physical insight can be gained by substituting Eq. (10) into the right-hand side of (14) and taking the limit as $\Delta y_1 \to 0$, noting that $\tau = \Delta y_1 / U_c$. This leads to

$$\ddot{Q}_{ij}(t) = \frac{\partial^2}{\partial t^2}\int_{V_0} T_{ij}(\mathbf{y}, t)\,d^3\mathbf{y} + \frac{\partial}{\partial t}\int_{S_0} U_c T_{ij}(\mathbf{y}, t)\,d^2\mathbf{y} \tag{15}$$

which shows clearly that the boundary correction to the volume quadrupole source calculated in a truncated domain V_0 is equivalent to the time derivative of the Lighthill stress fluxes across the exit boundary S_0, carried by the convecting eddies at velocity U_c. In other words, the net contribution from the missing acoustic source functions outside the integration domain can be approximated by a flux term evaluated on the exit surface. In the preceding derivation, the eddy convective velocity U_c is assumed to be parallel to the y_1 axis and S_0 is a plane surface perpendicular to the flow direction. If S_0 is a curved surface as, for example, defined by the normal mesh lines in the airfoil wake (Fig. 1), the projected area normal to y_1 is used. This semiempirical formulation can be generalized to the case of noncompact sources by modifying (7) accordingly. The volume quadrupole contribution to the far-field density disturbance $\rho - 1$, henceforth denoted as ρ_q, takes the form

$$\rho_q(\mathbf{x}, t) = \frac{M^4}{4\pi}\left[\frac{\partial^2}{\partial t^2}\int_{V_0} \frac{r_i r_j}{r^3} T_{ij}(\mathbf{y}, t - Mr)\,d^3\mathbf{y} + \frac{\partial}{\partial t}\int_{S_0} \frac{r_i r_j}{r^3} U_c T_{ij}(\mathbf{y}, t - Mr)\,d^2\mathbf{y}\right] \tag{16}$$

In aeroacoustic problems whose solutions are known to be time periodic, it is customary to conduct calculations in the frequency domain (see, for instance, Refs. 4 and 5). The corresponding expression for the quadrupole noise with a boundary correction is thus useful. By taking the Fourier time transform of Eq. (16) according to

$$\hat{\rho}_q(\mathbf{x}, \omega) = \int_{-\infty}^{\infty} \rho_q(\mathbf{x}, t) e^{-i\omega t}\,dt \tag{17}$$

one obtains

$$\hat{\rho}_q(\mathbf{x}, \omega) = -\frac{M^4}{4\pi}\left[\omega^2 \int_{V_0} \frac{r_i r_j}{r^3} \hat{T}_{ij}(\mathbf{y}, \omega) e^{iM\omega r}\,d^3\mathbf{y} + i\omega \int_{S_0} \frac{r_i r_j}{r^3} U_c \hat{T}_{ij}(\mathbf{y}, \omega) e^{iM\omega r}\,d^2\mathbf{y}\right] \tag{18}$$

Again, the corrective surface term accounting for the effect of escaping eddies is simple and readily computable along with the volume integral. The derivation, on the other hand, would be less straightforward if it were carried out in the frequency domain, where the physical significance of the boundary correction is not as obvious.

V. Results and Discussion

The simulated flowfield around the airfoil presented in Sec. II is two dimensional, implying constant properties along an infinite span. The acoustic formulation in Secs. III and IV, on the other hand, represents three-dimensional solutions to a forced, linear wave equation, and we are interested in the acoustic waves emitted from unit span based on the above formulation. Alternatively, one could consider a strictly two-dimensional problem by employing a two-dimensional version of the acoustic analogy, which can be derived easily by integrating the three-dimensional formulas along the infinite span.[3,19] The results are, however, of less physical relevance because in practical situations involving a long span, the near-field inevitably develops three-dimensionality, and thus the phase difference between the various radiating elements along the span cannot be ignored.

To illustrate the effect of boundary correction, Figs. 4a and 4b compare the time oscillations of the compact longitudinal quadrupole $\ddot{Q}_{11}$ calculated from Eq. (15), before and after the boundary correction term is added. In the calculations, it is assumed that $T_{ij} \approx v_i v_j$, an approximation justified by the relatively large

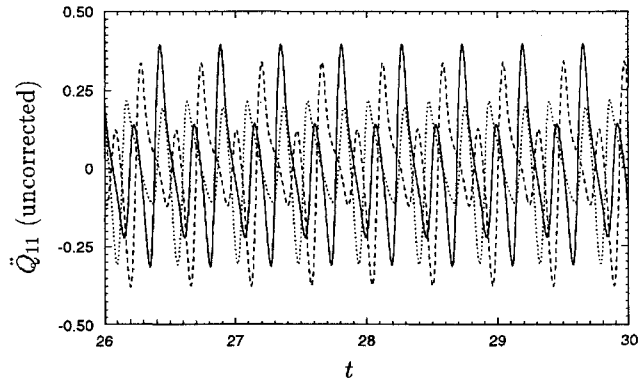

a) Without boundary correction

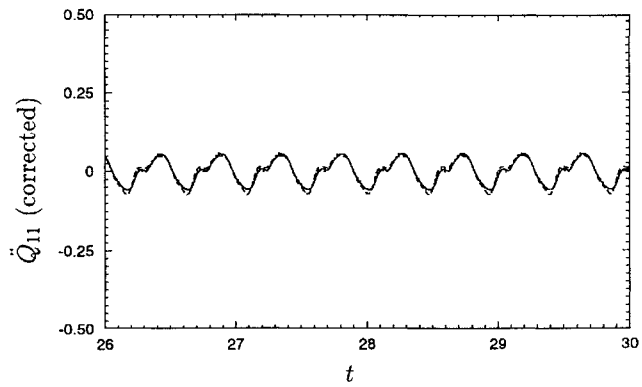

b) With boundary correction

Fig. 4 Longitudinal quadrupole $\ddot{Q}_{11}$ calculated from three different-sized source domains whose downstream boundaries are located at ——, $x_{1\max} \approx 2.59$; - - - -, $x_{1\max} \approx 2.89$; and ·····, $x_{1\max} \approx 3.21$. The airfoil angle of attack $\alpha = 5$ deg.

Reynolds number and small Mach number. The three curves represent evaluations based on three different-sized source domains whose downstream boundaries, defined by the normal mesh lines in Fig. 1, are 20 grid points apart. The maximum y_1 (x_1) coordinates of these exit surfaces are given by $y_{1\max} \approx 2.59$, 2.89, and 3.21, at the intersections with the branch cut. The primitive (uncorrected) Lighthill quadrupole, shown in Fig. 4a, is seen to exhibit a strong dependence on the downstream boundary location. After applying the corrections, the three curves are seen to converge as shown in Fig. 4b, indicating the physical noise source caused by vortex generation near the trailing edge, which is well captured within all three integration domains. In estimating the boundary Reynolds stress fluxes, a constant convective velocity $U_c = 0.90$ is used for all three surfaces. The corrective effects are found to be rather insensitive to the value of U_c, although a slight improvement has been observed by fine tuning the value of U_c based on the local convective velocity on each surface.

The same comparisons are made in Figs. 5 and 6 for quadrupoles $\ddot{Q}_{12}$ and $\ddot{Q}_{22}$, respectively, before and after the boundary correction. Like $\ddot{Q}_{11}$, the corrected lateral quadrupole $\ddot{Q}_{12}$ is nearly independent of the exit boundary location (Fig. 5b). A comparison of Figs. 6a and 6b indicates a drastic reduction in the boundary errors for $\ddot{Q}_{22}$ as well. In fact its after-correction magnitude reduces to merely $\frac{1}{8}$ of the precorrection value, approximately. Although the three curves in Fig. 6b still show significant disagreement in the higher-frequency components, a basic oscillatory pattern at the vortex shedding frequency has emerged. The residual errors may arise because of the crude approximation concerning the Lighthill stress flux across the exit boundary, based on a single convective velocity U_c. In reality, the transport of the Lighthill stress, or the instantaneous Reynolds stress, may be spatially nonuniform and dependent on eddy scales. These effects must be taken into consideration if further improvement is to be made.

An example of boundary corrections applied to an aperiodic source is given in Figs. 7a and 7b. The quadrupole $\ddot{Q}_{11}$ is obtained

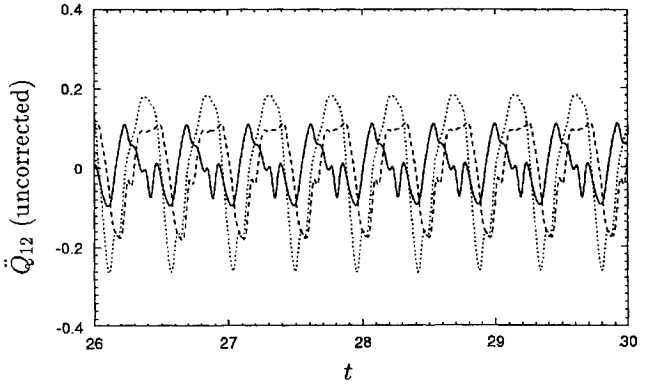

a) Without boundary correction

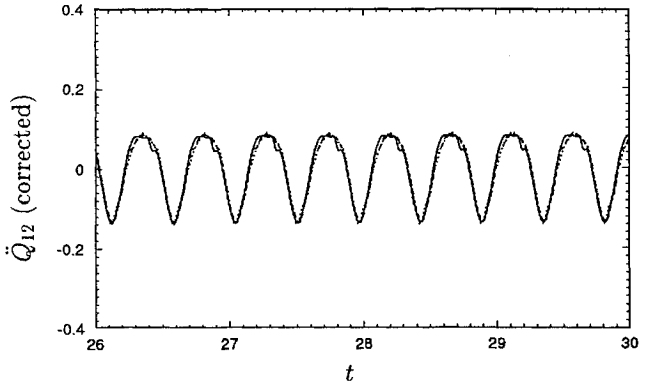

b) With boundary correction

Fig. 5 Lateral quadrupole $\ddot{Q}_{12}$ calculated from three different-sized source domains whose downstream boundaries are located at ——, $x_{1\max} \approx 2.59$; - - - -, $x_{1\max} \approx 2.89$; and ·····, $x_{1\max} \approx 3.21$. The airfoil angle of attack α = 5 deg.

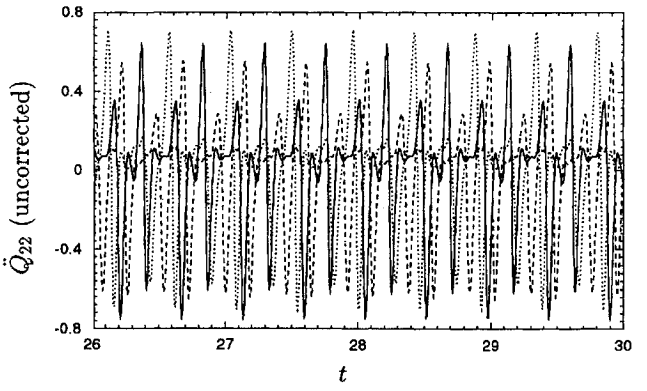

a) Without boundary correction

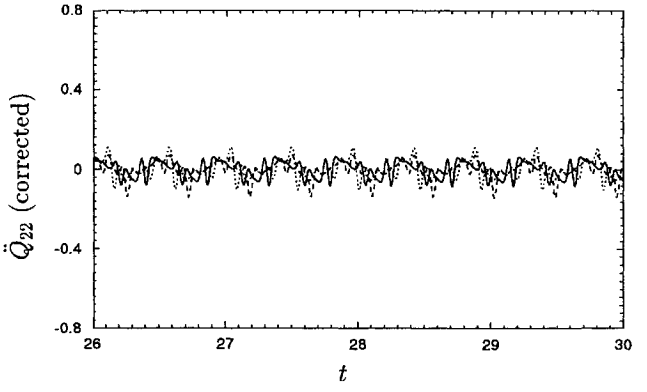

b) With boundary correction

Fig. 6 Longitudinal quadrupole $\ddot{Q}_{22}$ calculated from three different-sized source domains whose downstream boundaries are located at ——, $x_{1\max} \approx 2.59$; - - - -, $x_{1\max} \approx 2.89$; and ·····, $x_{1\max} \approx 3.21$. The airfoil angle of attack α = 5 deg.

based on the near-field simulation data for the case of $\alpha = 8$ deg. Again, three exit boundaries passing the same $y_{1\max}$ stations on the branch cut as in Figs. 4–6 are used to illustrate the dominant impact of boundary errors in the source calculation, as shown in Fig. 7a. The corrected $\ddot{Q}_{11}$ source terms in Fig. 7b, as well as the other two quadrupole components not shown, compare well despite the nonharmonic nature of the signals. This is important because the main advantage of solving aeroacoustic problems in the time domain lies in its ability to treat arbitrary, nonperiodic signals. In comparison with the $\alpha = 5$ deg case (Fig. 4b), Fig. 7b indicates higher-amplitude, lower-frequency acoustic phenomena corresponding to the stronger vortices shed at a slower rate in the near field. The eddy convective velocity U_c in Eq. (15) is found to be best approximated by 1.0.

In the event that the source integration domain is not small in comparison to the acoustic wavelength, retarded-time variations in the source region become significant. The boundary corrections are applied directly to the far-field density according to Eq. (16). To examine the efficacy of this more general approach, an efficient integration-interpolation method has been developed for the evaluation of the volume and surface integrals in relations (7) and (16). The scheme treats each near-field computational cell or boundary element as an individual acoustic source. At each simulation time step t_n, the future time $\sigma_n = t_n + M|x-y|$, at which the emitted acoustic signal reaches the far-field position x, is calculated. The scheme then locates in the discretized far-field time series the point straddled by σ_{n-1} and σ_n and interpolates linearly on the integrands to find their contributions to the far-field density at that time. The total density history at the observation point is obtained by summing contributions from all of the source elements and accumulating over all the time steps. The acoustic integration scheme, which is second order accurate in both space and time, uses the same time step size as for the near-field simulation. The extra memory requirement is minimal because only the contracted integrands (after summations

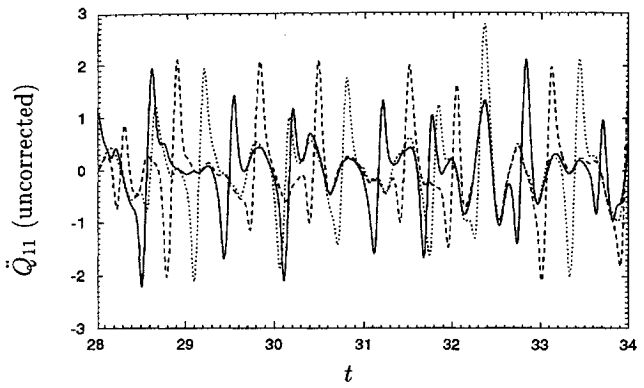

a) Without boundary correction

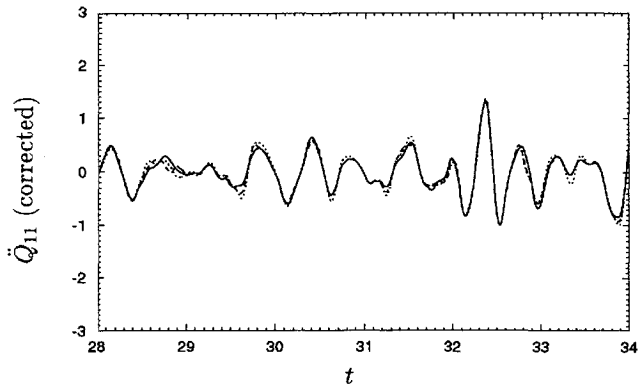

b) With boundary correction

Fig. 7 Same as in Fig. 4, except that the airfoil angle of attack α = 8 deg.

over i and j) in the volume and surface integrals need to be stored at an additional time level.

Figures 8a and 8b contrast the far-field acoustic pressure signals due to quadrupole radiation for the case of $\alpha = 5$ deg, evaluated in the same integration domains as in Figs. 4–6, before and after the boundary corrections. The quadrupole pressure ($p_q \equiv \gamma\rho_q$, renormalized by the mean freestream pressure) is calculated directly from Eq. (16) with full account of the retarded time, for a given far-field position $|x| = 50$, $\theta = 30$ deg, where θ defines the angle measured counterclockwise from the downstream x_1 axis. The freestream Mach number $M = 0.2$. The three p_q curves corresponding to the three different exit boundaries compare rather well after corrections are applied. The discrepancy, in the form of higher-frequency oscillations, is due mainly to the T_{22} source component whose boundary effect is particularly difficult to eradicate, as in the compact source case shown in Fig. 6.

The retarded-time effect is illustrated in Figs. 9a and 9b for $M = 0.02$ and 0.2, respectively, by comparing the computational results with and without using the compact source approximation. Figures 9a and 9b again plot the quadrupole contribution to the acoustic pressure for $\alpha = 5$ deg, at $|x| = 200$ and $\theta = 30$ deg. The solid lines are obtained using Eq. (16), whereas the dashed lines are based on the compact source formulas (8) and (15). Both have been subjected to the appropriate boundary corrections, denoted as c_q and plotted separately in Figs. 10a and 10b. The residual boundary errors are of relative magnitude similar to that in Fig. 8b. The integration domain employed is the smallest among the three used earlier. As expected, the retarded-time effect is negligibly small at $M = 0.02$ and becomes somewhat significant at $M = 0.2$. In the latter case the noncompact formulation produces stronger radiation because of less cancellation among signals from different source elements. From Figs. 9a and 9b one observes little phase difference between the compact and noncompact solutions, suggesting that the acoustic source is centered very close to the origin of the coordinate $\boldsymbol{x}$, which, in the acoustic calculations, is defined at the trailing edge. In contrast, the boundary correction terms show an appreciable phase difference for $M = 0.02$ (cf. Fig. 10a) and a large phase difference for $M = 0.2$

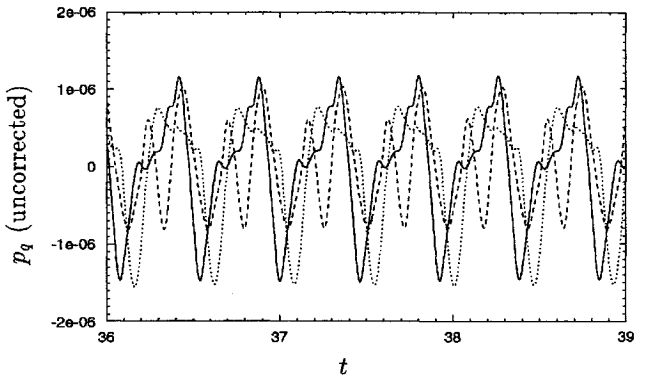

a) Without boundary correction

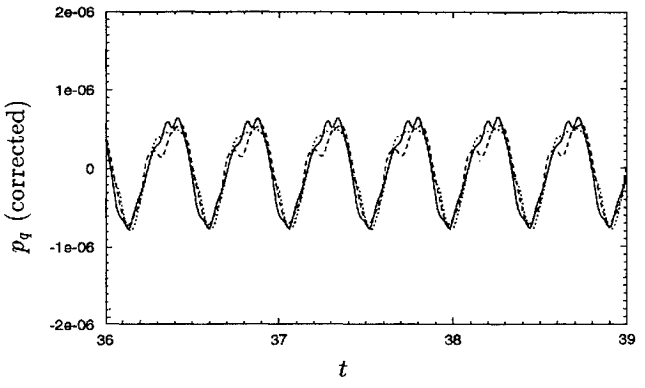

b) With boundary correction

Fig. 8 Acoustic pressure at $|x| = 50$, $\theta = 30$ deg due to quadrupole radiation, calculated from Eq. (16) using the same three integration domains as in Figs. 4–6. The airfoil is flying at $M = 0.2$ and $\alpha = 5$ deg.

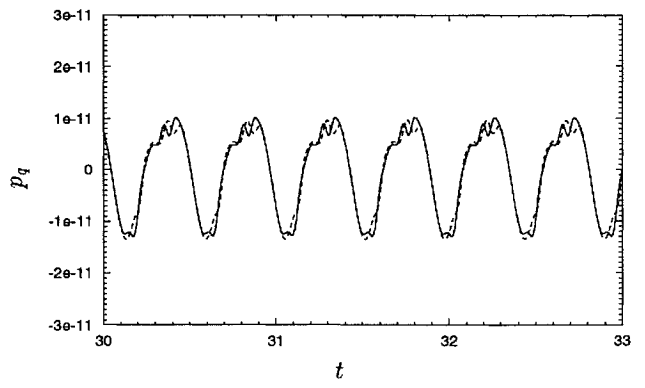

a) $M = 0.02$

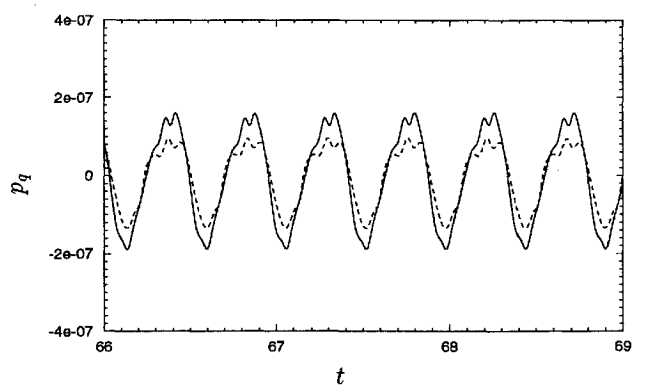

b) $M = 0.2$

Fig. 9 Acoustic pressure at $|x| = 200$, $\theta = 30$ deg due to quadrupole radiation, calculated based on ——, noncompact and - - - -, compact source formulations. The airfoil angle of attack α = 5 deg.

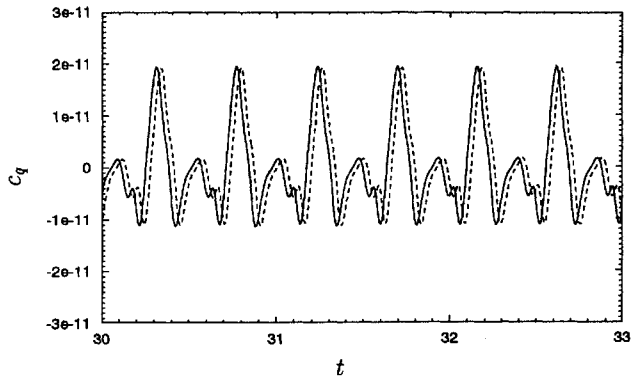

a) $M = 0.02$

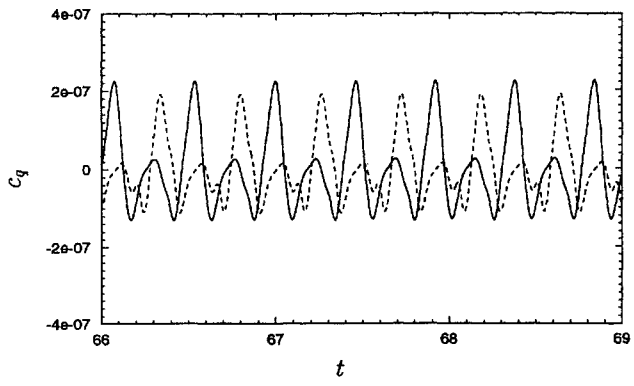

b) $M = 0.2$

Fig. 10 Boundary corrections to the acoustic pressure at $|x| = 200$, $\theta = 30$ deg, calculated based on ——, noncompact and - - - -, compact source formulations. The airfoil angle of attack $\alpha = 5$ deg.

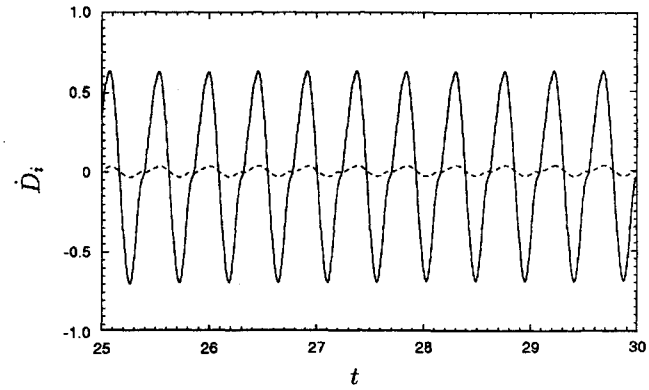

a) $\alpha = 5$ deg

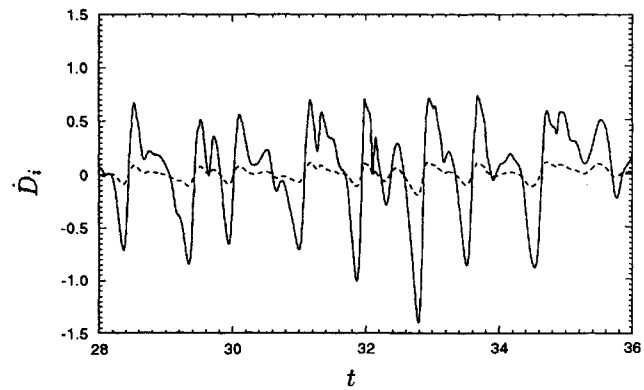

b) $\alpha = 8$ deg

Fig. 11 Acoustic dipoles on the airfoil surface, calculated from Eq. (9): - - - -, $\dot{D}_1$ (drag dipole) and ——, $\dot{D}_2$ (lift dipole).

(cf. Fig. 10b), because of the finite separation between the exit boundary and the trailing edge and the associated retarded time differences.

In the examples described in Figs. 8 and 9, the active source (vortex shedding region) is only slightly noncompact, even at $M = 0.2$. On the other hand, the source integration domains, containing 6–10 eddies depending on the exit boundary selection, are fairly noncompact in this case. Hence a valid test is provided for the general boundary treatment method [Eq. (16)] as well as the numerical integration scheme with retarded-time variations. The integration scheme is shown to be capable of providing adequate cancellations among signals from the passive convection region to form a converged solution regardless of the domain size. In addition, the good agreement with the compact source solution at the extremely low Mach number $M = 0.02$ shows that the scheme introduces negligible temporal interpolation error and provides the correct phase relationship among signals from the active source elements when the retarded-time differences are small.

A comment is in order concerning the selection of the integration boundary S_0. In principle, S_0 can be placed anywhere so long as the active noise source is enclosed within the source integration domain. From a computational standpoint, however, the velocity field in the vicinity of the outflow boundary for the Navier–Stokes simulation is somewhat distorted, due to the use of the approximate outflow boundary condition. The nonphysical eddy distortion may serve as another source of spurious noise if it is included in the calculation. For this reason, we always choose smaller source integration domains than the actual flow simulation domain, by placing S_0 at least 15 grid points upstream from the computational outflow boundary.

Accurate evaluations of the quadrupole sound require that the solutions be independent on all the boundaries enclosing the source region. In addition to tests with the exit boundary location, discussed earlier, we have repeated the calculations after the outer (C-shaped) boundary is moved inward by 10 grid points. No appreciable change was observed in the resulting acoustic signals.

Finally, the surface acoustic sources due to the unsteady compressive stress exerted by the airfoil were evaluated and compared with the volume quadrupoles. Under the condition that the airfoil chord is small relative to the acoustic wavelength, the compact solution form (8) and (9) applies. The calculated point dipole components are depicted in Figs. 11a and 11b for the cases of $\alpha = 5$ and 8 deg, respectively. Both the pressure and viscous stress are included in the calculations of p_{ij}. The viscous contribution to the lift dipole $\dot{D}_2$ is negligibly small. Its effect on the drag dipole $\dot{D}_1$, on the other hand, reaches approximately 27% in magnitude relative to the pressure contribution, for the case of $\alpha = 5$ deg. Overall, the lift dipole is much stronger than the drag dipole, and both amplify with increasing angle of attack. Relative to the Reynolds-stress quadrupole components calculated earlier, $\dot{D}_2$ is of larger or comparable magnitude and thus dominates the overall radiation, given that its coefficient in (8) is $O(M^{-1})$ larger than that of the quadrupole terms. At shallow θ angles, the quadrupole sources still play a role because the magnitude of $\dot{D}_1$ is also small. However, in this region one also needs to account for the wave modification due to refraction and scattering by the wake flow, not considered in this study.

As a related matter, we note that the Curle integral,[10] evaluated based on an incompressible near field, does not provide an adequate description of the effect of aeroacoustic scattering by large, acoustically noncompact airfoils. If the chord length is comparable with or exceeds one acoustic wavelength, the compressibility effect on the surface integral is nonnegligible. Surface scattering, particularly near the trailing edge, can cause a considerable increase in the radiated power and a concomitant alteration in directivity. Both theory[20–22] and experimental evidence[23] suggest a nonmultipole character for the scattered fields of hard surfaces with a sharp edge. In the limiting case of scattering by a semi-infinite thin plane, the far-field intensity is known to be dependent on the fifth power of the fluid velocity and to have a $\sin^2(\theta/2)$ directivity pattern. To predict the edge scattering noise, one must take into account the acoustic interaction with the airfoil surface, by using either compressible flow simulations or the appropriate hard-wall Green's function in

a Lighthill-analogy-based calculation. This will be the subject of a future investigation.

VI. Conclusions

In acoustic-analogy-based calculations of aerodynamic sound, it is important to distinguish the active source region, where production of the unsteady Reynolds stress takes place, from passive regions characterized by the convective motion of eddies. The former should always be enclosed within the domain of source integration, whereas the latter may be truncated, provided that an adequate account of the effect of eddies crossing the permeable integration boundary is provided.

This paper illustrates the necessity for, and means of, boundary corrections through a paradigm problem of airfoil vortex shedding. It demonstrates that the spurious noise generated by the exit boundary in the airfoil wake is due to the time variation of the unsteady momentum fluxes across the boundary, carried by the escaping eddies. For a class of problems in which eddies (organized structures) leave (enter) the source integration domain at a nearly constant speed, the spurious boundary noise can be eliminated or reduced drastically by the correction terms in relations (14–18). This approach allows a quantitative evaluation of the radiated quadrupole noise, which has rarely been done in the past.

In the case of vortex shedding from a small airfoil, computational results suggest that the volume quadrupole noise is small in the low-Mach-number limit, in comparison to the prevalent lift and drag dipole noise emitted from the airfoil surface. The techniques developed in this study are equally applicable to other flow configurations, such as jets and mixing layers, in which the volume acoustic sources provide the dominant contribution to the far-field noise.

Acknowledgments

This work was supported by the U.S. Office of Naval Research under Grant N00014-95-1-0221. Computations were carried out on the Numerical Aerodynamic Simulation facilities at NASA Ames Research Center. We gratefully acknowledge H. Choi and H.-J. Kaltenbach for providing the Navier–Stokes code and related assistance and G. M. Lilley and K. Shariff for many stimulating discussions.

References

[1]Lighthill, M. J., "On Sound Generated Aerodynamically: I. General Theory," *Proceedings of the Royal Society of London, Series A: Mathematical and Physical Sciences*, Vol. 211, No. 1107, 1952, pp. 564–587.

[2]Crow, S. C., "Aerodynamic Sound Emission as a Singular Perturbation Problem," *Studies in Applied Mathematics*, Vol. 49, No. 1, 1970, pp. 1–44.

[3]Mitchell, B. E., Lele, S. K., and Moin, P., "Direct Computation of the Sound from a Compressible Co-rotating Vortex Pair," *Journal of Fluid Mechanics*, Vol. 285, Feb. 1995, pp. 181–202.

[4]Mitchell, B. E., Lele, S. K., and Moin, P., "Direct Computation of the Sound Generated by Vortex Pairing in an Axisymmetric Jet," AIAA Paper 95-0504, Jan. 1995.

[5]Mankbadi, R. R., Hayder, M. H., and Povinelli, L. A., "Structure of Supersonic Jet Flow and Its Radiated Sound," *AIAA Journal*, Vol. 32, No. 5, 1994, pp. 897–906.

[6]Wang, M., Lele, S. K., and Moin, P., "Sound Radiation During Local Laminar Breakdown in a Low Mach Number Boundary Layer," *Journal of Fluid Mechanics*, Vol. 319, July 1996, pp. 197–218.

[7]Sarkar, S., and Hussaini, M. Y., "Computation of the Sound Generated by Isotropic Turbulence," Inst. for Computer Applications in Science and Engineering, ICASE Rept. 93-74, NASA Langley Research Center, Hampton, VA, Oct. 1993.

[8]Crighton, D. G., "Computational Aeroacoustics for Low Mach Number Flows," *Computational Aeroacoustics*, ICASE/NASA LaRC Series, edited by J. C. Hardin and M. Y. Hussaini, Springer–Verlag, New York, 1993, pp. 50–68.

[9]Tam, C. K. W., "Computational Aeroacoustics: Issues and Methods," *AIAA Journal*, Vol. 33, No. 10, 1995, pp. 1788–1796.

[10]Curle, N., "The Influence of Solid Boundaries upon Aerodynamic Sound," *Proceedings of the Royal Society of London, Series A: Mathematical and Physical Sciences*, Vol. 231, No. 1187, 1955, pp. 505–514.

[11]Phillips, O. M., "The Intensity of Aeolian Tones," *Journal of Fluid Mechanics*, Vol. 1, Pt. 6, 1956, pp. 607–624.

[12]Adachi, S., Ishii, K., Akishita, S., and Kuwahara, K., "Computation of Aerodynamic Sound Radiation from Flows Past a Wing," DGLR/AIAA 14th Aeroacoustics Conf., DGLR/AIAA Paper 92-02-157, Aachen, Germany, May 1992.

[13]Haruna, S., Hashiguchi, M., Kamimoto, I., and Kuwahara, K., "Numerical Study of Aerodynamic Noise Radiated from a Three-Dimensional Wing," *SAE Transactions*, Vol. 101, Sec. 6, 1992, pp. 389–402 (SAE Paper 920341).

[14]Ffowcs Williams, J. E., and Hawkings, D. L., "Sound Generation by Turbulence and Surfaces in Arbitrary Motion," *Philosophical Transactions of the Royal Society of London, Series A: Mathematical and Physical Sciences*, Vol. 264, No. 1151, 1969, pp. 321–342.

[15]Choi, H., "Toward Large Eddy Simulation of Turbulent Flow over an Airfoil," *Annual Research Briefs—1993*, Center for Turbulence Research, Stanford Univ./NASA Ames Research Center, Stanford, CA, 1993, pp. 145–149.

[16]Pauley, L. L., Moin, P., and Reynolds, W. C., "The Structure of Two-Dimensional Separation," *Journal of Fluid Mechanics*, Vol. 220, Nov. 1990, pp. 397–411.

[17]Pulliam, T. H., "Low Reynolds Number Numerical Solutions of Chaotic Flows," AIAA Paper 89-0123, Jan. 1989.

[18]Goldstein, M. E., *Aeroacoustics*, McGraw–Hill, New York, 1976, Chap. 4.

[19]Wang, M., "Sound Radiation due to Boundary Layer Transition," *Annual Research Briefs—1993*, Center for Turbulence Research, Stanford Univ./NASA Ames Research Center, Stanford, CA, 1993, pp. 299–312.

[20]Ffowcs Williams, J. E., and Hall, L. H., "Aerodynamic Sound Generation by Turbulent Flow in the Vicinity of a Scattering Half Plane," *Journal of Fluid Mechanics*, Vol. 40, Pt. 4, 1970, pp. 657–670.

[21]Crighton, D. G., and Leppington, F. G., "On the Scattering of Aerodynamic Noise," *Journal of Fluid Mechanics*, Vol. 46, Pt. 3, 1971, pp. 577–597.

[22]Howe, M. S., "A Review of the Theory of Trailing Edge Noise," *Journal of Sound and Vibration*, Vol. 61, No. 3, 1978, pp. 437–465.

[23]Brooks, T. F., and Hodgson, T. H., "Trailing Edge Noise Prediction from Measured Surface Pressures," *Journal of Sound and Vibration*, Vol. 78, No. 1, 1981, pp. 69–117.